Determination of ^{53}Mn(n, xp) cross sections using the surrogate reaction ratio method

Ramandeep Gandhi,[1,*] B. K. Nayak,[1,2] S. V. Suryanarayana,[1] A. Pal,[1,2] G. Mohanto,[1] S. De,[1] A. Parihari,[1,†] A. Kundu,[1,2] P. C. Rout,[1,2] S. Santra,[1,2] K. Mahata,[1,2] B. Srinivasan,[1] E. T. Mirgule,[1] and J. Pandey[3]

[1]*Nuclear Physics Division, Bhabha Atomic Research Centre, Mumbai 400085, India*

[2]*Homi Bhabha National Institute, Anushaktinagar, Mumbai 400094, India*

[3]*Department of Physics, G.B. Pant University of Agriculture and Technology, Pantnagar, Uttarakhand 263145, India*

(Received 16 July 2019; revised manuscript received 27 September 2019; published 18 November 2019)

The ^{54}Mn* (surrogate of $n + ^{53}$Mn) and ^{61}Ni* (surrogate of $n + ^{60}$Ni) compound systems have been populated at overlapping excitation energies by transfer reactions ^{52}Cr(^{6}Li, α)^{54}Mn* at $E_{\rm lab} = 33.0$ MeV and ^{59}Co(^{6}Li, α)^{61}Ni* at $E_{\rm lab} = 40.5$ MeV, respectively. The proton decay probabilities of the compound systems have been determined by measuring evaporated protons at backward angles in coincidence with projectilelike fragments detected around the grazing angle. The ^{53}Mn(n, xp) cross sections in the equivalent neutron energy range of 8.2–16.4 MeV have been determined within the framework of the surrogate reaction ratio method using ^{60}Ni(n, xp) cross-section values from the literature as a reference. The measured ^{53}Mn(n, xp) cross-section values are found to be consistent with the predictions of the TALYS-1.8 statistical model code using microscopic level densities and results of various evaluated nuclear data libraries: EAF-2010, ROSFOND-2010, and JEFF-3.3 within the experimental uncertainties.

DOI: 10.1103/PhysRevC.100.054613

I. INTRODUCTION

Improved and accurate nuclear data are of utmost importance for the design of advanced reactor systems based on nuclear fusion and fission reactions [1]. The intense flux of high-energy neutrons produced in a fusion reactor through a D + T reaction irradiates the structural materials inducing nuclear reactions. The neutron induced nuclear reactions that produce gaseous products, such as hydrogen (H) and helium (He) through (n, xp) and $(n, x\alpha)$ reactions, lead to swelling and embrittlement of structural material of the reactor. Additionally, the high-energy neutron flux causes radiation defects by atomic displacement and transmutations, which modifies the physical properties of the structural materials. Furthermore, due to continuous bombardment of neutrons many long-lived radionuclides are produced through neutron capture by various stable nuclei present in the structural materials, such as Cr, Fe, and Ni. Some of the long-lived radionuclides produced in the mass region of 50–60 are ^{53}Mn($T_{1/2} = 3.74 \times 10^6$ yr), ^{55}Fe($T_{1/2} = 2.73$ yr), ^{60}Fe($T_{1/2} = 1.5 \times 10^6$ yr), ^{60}Co($T_{1/2} = 5.27$ yr), ^{59}Ni($T_{1/2} = 7.6 \times 10^4$ yr), and ^{63}Ni($T_{1/2} = 100.1$ yr). The experimental data on (n, xp) and $(n, x\alpha)$ cross sections with the above long-lived radionuclei are very important for the safety and design analysis of the reactor systems [2–4].

Out of the long-lived radionuclei mentioned above, ^{53}Mn is produced during reactor operation predominantly via ^{54}Fe(n, np), ^{54}Fe(n, d), and ^{54}Fe$(n, 2n)^{53}$Fe(β^+) reactions with respective neutron threshold energies of 9, 6.8, and 13.6 MeV [5–7]. The major pathways of ^{53}Mn formation in a typical fusion reactor are depicted in Fig. 1. The (n, γ), (n, p), and (n, α) reaction channels for ^{53}Mn have positive Q values of 8.938, 1.379, and 0.180 MeV, respectively. The significant growth of ^{53}Mn will result in the production of hydrogen and helium via (n, xp) and $(n, x\alpha)$ reactions. But, for ^{53}Mn, there is no experimental data available in the literature on (n, xp) and $(n, x\alpha)$ cross sections. So, it will be of considerable interest to measure these cross sections in order to estimate the contribution of hydrogen and helium productions involving the ^{53}Mn target.

^{53}Mn is not a naturally occurring isotope due to which direct measurements of ^{53}Mn(n, xp) and ^{53}Mn$(n, x\alpha)$ cross sections are difficult. In our earlier work [8,9], we have determined ^{55}Fe(n, p) and ^{59}Ni(n, xp) cross sections by the surrogate reaction ratio method where a fixed beam energy populates the residual nuclei over a wide range of excitation energies, which allows us to determine the cross sections over a range of equivalent neutron energies.

In the present paper, the ^{53}Mn(n, xp) reaction cross sections have been measured by the ^{52}Cr(^{6}Li, α)^{54}Mn* transfer reaction as a surrogate of the $n + ^{53}$Mn reaction. The ^{60}Ni(n, xp) reaction cross sections have been used as a reference by populating the ^{61}Ni* compound system through the ^{59}Co(^{6}Li, α)^{61}Ni* transfer reaction at similar excitation energies. The proton decay probabilities of compound systems ^{54}Mn* and ^{61}Ni* are determined by measuring the evaporated protons at backward angles in coincidence with projectilelike

*ramangandhipu@gmail.com

†Current address: Inter University Accelerator Centre, New Delhi 110067, India.

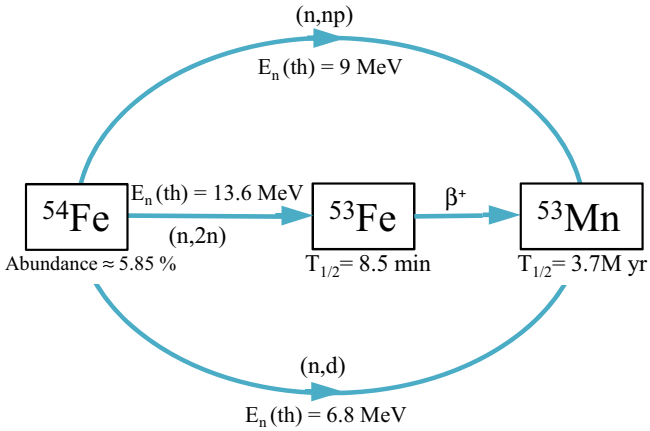

FIG. 1. Major pathways of ^{53}Mn formation in a typical fusion reactor.

fragment (PLF) α around the grazing angle. The paper has been organized as follows. The details of the experimental setup and data analysis are given in Sec. II. Results and discussions are given in Sec. III, followed by the summary and conclusions in Sec. IV.

II. EXPERIMENTAL DETAILS AND DATA ANALYSIS

Measurements have been carried out at the BARC-TIFR Pelletron Accelerator Facility in Mumbai. ^{6}Li beams were bombarded on a freshly prepared self-supporting target of natural Cr (abundance ^{52}Cr $\approx$ 84%) of thickness $\approx$578 μg/cm^2 and ^{59}Co (abundance $\approx$100%) of thickness $\approx$500 μg/cm^2 at incident energies of $E_{\rm lab}$ = 33.0 and 40.5 MeV, respectively. The schematic of the experimental setup is shown in Fig. 2. For the present experiment, the surrogate reactions of interest, their ground-state Q-values ($Q_{\rm gg}$), the compound nuclei (CN) formed, neutron separation energies (S_n), and corresponding equivalent neutron induced reactions are listed in Table I.

TABLE I. Surrogate reactions investigated in the present experiment, their ground-state Q-values ($Q_{\rm gg}$), the CN formed, neutron separation energies (S_n), and corresponding equivalent neutron induced reactions.

$E^{^6{\rm Li}}_{\rm beam}$ (MeV)	Surrogate reaction	$Q_{\rm gg}$ (MeV)	CN	S_n (MeV)	Equivalent neutron induced reaction
33	^{52}Cr(^{6}Li, α)^{54}Mn*	11.8	^{54}Mn*	8.939	^{53}Mn(n, xp)
40.5	^{59}Co(^{6}Li, α)^{61}Ni*	13.65	^{61}Ni*	7.820	^{61}Ni(n, xp)

The projectilelike fragments were identified by a silicon surface barrier (SSB) $\Delta E - E$ detector telescope with thicknesses of $\Delta E \approx 150$ μm and $E \approx 1$ mm. The telescope was mounted at 25° with respect to the beam direction around the grazing angle. A typical two-dimensional energy calibrated plot of ΔE versus $E_{\rm total}$ (total energy) clearly identifies different PLFs, i.e., proton, deuteron, triton, and α particles as shown in Fig. 3. The typical energy resolution of the α particle detected in telescope (T) is $\approx$150 keV. The formation of compound nuclei ^{54}Mn* and ^{61}Ni* in transfer reactions ^{52}Cr(^{6}Li, α)^{54}Mn* and ^{59}Co(^{6}Li, α)^{61}Ni*, respectively, were identified by outgoing PLF(α).

Two large area Si strip detector telescopes (S1 and S2) were mounted at backward angles 120° and 150° with respect to beam direction each having an angular opening of ~16° to detect evaporated particles (e.g., p, d, t, and α) from the compound nuclei ^{54}Mn* and ^{61}Ni* in coincidence with the PLF(α). Each Si strip telescope consists of a ΔE detector of thickness $\approx$60 μm and an E detector of thickness of $\approx$1500 μm, each having an active area of 50 × 50 mm^2. Each strip detector has 16 vertical strips of size 3.1 × 50.0-mm^2 each. A typical two-dimensional correlation plot of ΔE versus

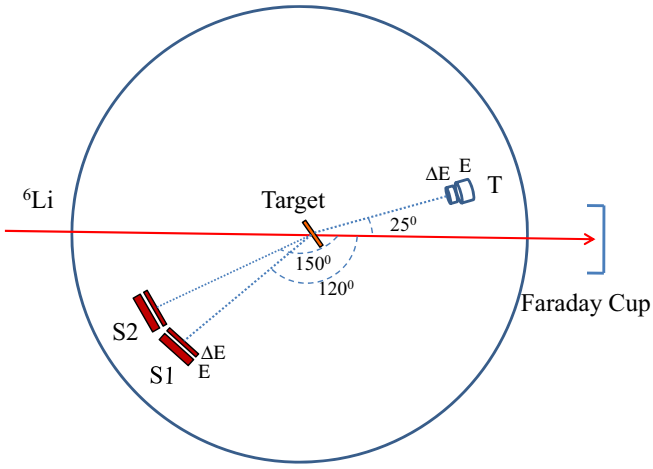

FIG. 2. A schematic of experimental setup inside a 1.5-m diameter scattering chamber. Here, "T" is a particle telescope for detecting the PLFs placed at a distance of 17 cm from the target center. The Si strip telescopes S1 and S2 (placed at 21 cm from the target center) have been used to identify the evaporated particles, such as p, d, t, and α at backward angles.

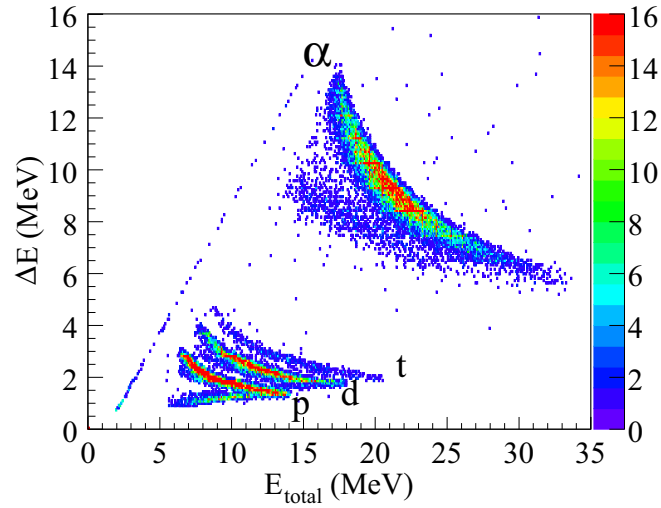

FIG. 3. A typical correlation plot of ΔE versus $E_{\rm total}$ (total energy) corresponding to the particles detected in the Si surface barrier detector telescope (T) placed at 25° for the ^{6}Li + ^{52}Cr reaction at $E_{\rm lab}$ = 33.0 MeV.

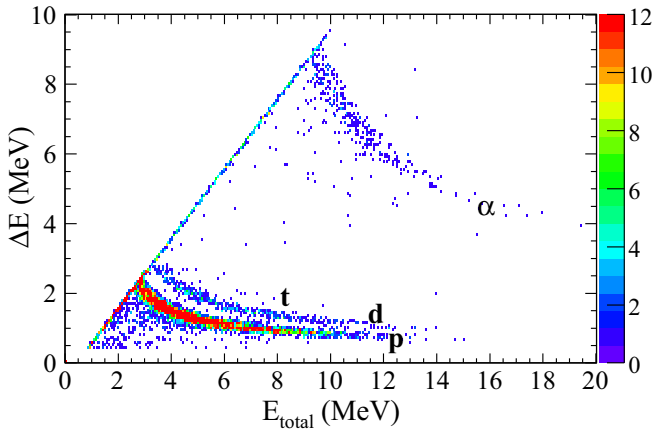

FIG. 4. A typical plot of ΔE versus E_{total} (total energy) obtained from one of the 32 $\Delta E - E$ strip combinations placed at backward angles for the ^{6}Li + ^{52}Cr reaction at $E_{\text{lab}} = 33.0$ MeV.

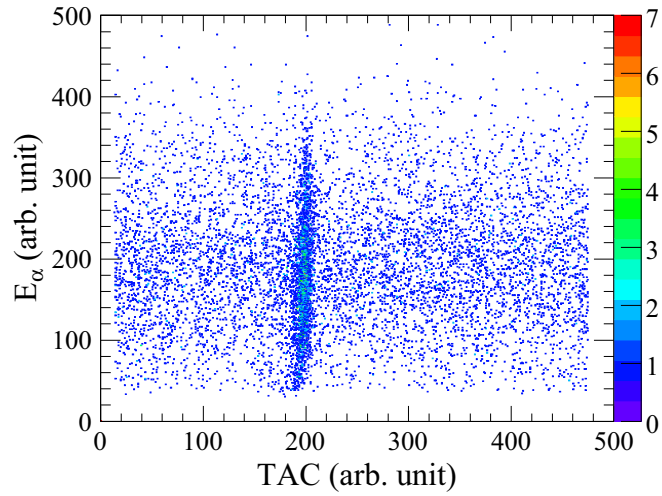

FIG. 5. A typical two-dimensional plot of energy of α particle (E_α) detected in telescope T versus the TAC between the α particles detected in the single telescope T and the evaporated protons detected in the strip detector telescope S1 for the ^{6}Li + ^{52}Cr reaction measured at $E_{\text{lab}} = 33.0$ MeV.

E_{total}, obtained from one of the 32 $\Delta E - E$ strip combinations, shown in Fig. 4, clearly identifies the particles of H isotopes (p, d, t) and ^{4}He. Typical energy resolution of a strip detector is $\approx$100 keV.

In-beam energy calibration of the SSB telescope (T) and strip telescopes (S1 and S2) was carried out using the known excited states of ^{16}O* formed in the ^{12}C(^{6}Li, d) ^{16}O* reaction at $E_{\text{lab}} = 18$ MeV. Energy calibration was also performed by the known energies of α particles from a Pu-Am α source. The time correlations between the detected particles in the T detector and the subsequent decay particles in detector S1 or S2 were recorded through a time-to-amplitude converter (TAC). A typical two-dimensional plot of the energy of an α particle (E_α) detected in telescope T versus TAC between the particles detected in T and evaporated protons detected in S1 for the ^{6}Li + ^{52}Cr reaction at $E_{\text{lab}} = 33.0$ MeV is shown in Fig. 5.

The excitation energy spectra of targetlike compound systems of ^{54}Mn* and ^{61}Ni* were determined from the "event by event analysis," employing two-body kinematics for the PLF α channel. The excitation energy spectra obtained for ^{54}Mn* and ^{61}Ni* compound nuclei in coincidence with evaporated protons are shown in Figs. 6(a) and 6(b), respectively. The respective excitation energy spectra corresponding to the singles PLF (α) are shown in Figs. 6(c) and 6(d). These spectra are generated for an excitation energy bin width of 0.5 MeV, leading to an uncertainty in excitation energy of $\pm$0.25 MeV. The compound systems ^{54}Mn* and ^{61}Ni* are found to be populated at overlapping excitation energies in the range of $\approx$17–25 MeV in the ^{52}Cr(^{6}Li, α) ^{54}Mn* reaction at E_{lab} (^{6}Li) = 30.0 MeV and ^{59}Co(^{6}Li, α) ^{61}Ni* reaction at E_{lab} (^{6}Li) = 40.5 MeV, respectively. The overlapping excitation energy range is marked by two dotted lines as shown in Fig. 6.

The proton decay (particle evaporation) probabilities from ^{54}Mn* and ^{61}Ni* compound nuclei produced in the transfer reactions are obtained using the following relation:

$$\mathrm{P}^{\mathrm{CN}}_{\alpha,p}(E^*) = \frac{N_{\alpha,p}(E^*)}{N_\alpha(E^*)}. \quad (1)$$

N_α and $N_{\alpha,p}$ denote the singles (α) and coincidence counts (between PLF α and evaporated p), obtained corresponding to excitation energy (E^*).

To confirm that protons are emitted by evaporation of the compound nuclei ^{54}Mn*, the proton spectrum has been compared with the statistical model code PACE4 [10] predictions at excitation energy $E^* = 22.5$ MeV. The evaporation proton spectrum from the compound system ^{54}Mn* at $E^* =$ 22.5 MeV, in coincidence with PLF(α) along with PACE4 predictions, is shown in Fig. 7. The predictions of PACE4 calculations and experimental proton spectrum compare well, indicating its compound nuclear evaporation nature. The angular momentum acquired by the excited compound system due to deuteron capture by the target nucleus is known to have a negligible effect on proton decay probabilities. In our recent work [9], we investigated the dependence of "compound nucleus angular momentum" on the "decay probability of the evaporated protons." When the projectilelike or beamlike fragments are emitted at two different angles (25° and 35°), they correspond to the population of excited compound nuclei at two different angular momenta. The proton decay probabilities were obtained separately for the two cases as a function of excitation energy of the composite nucleus and were found to be in good agreement with each other. It implies that the effect of the difference in angular momentum of the excited compound nucleus on proton decay probabilities that determine the (n, xp) cross section is negligible. Furthermore, an isotropic distribution of evaporated protons in the center of mass (by S1 and S2 detectors) in the angular range of $\approx$110°–160°, in coincidence with PLF(α) is also observed in the present paper.

The proton decay probabilities $P_p^{^{54}\mathrm{Mn}}(E^*)$ and $P_p^{^{61}\mathrm{Ni}}(E^*)$ of the excited compound systems ^{54}Mn* and ^{61}Ni* corresponding to the desired and reference reactions, have been determined in steps of 1.0-MeV excitation energy bin using

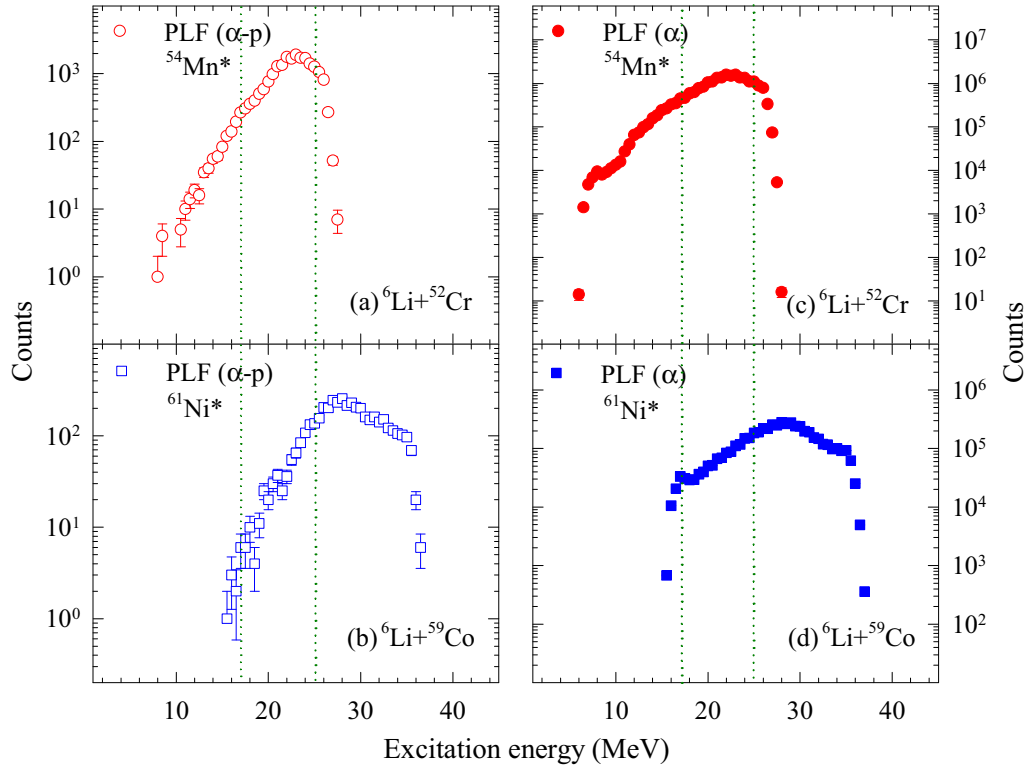

FIG. 6. Excitation energy spectra of the targetlike fragments produced in the ^{6}Li + ^{52}Cr and ^{6}Li + ^{59}Co reactions corresponding to PLF α with [(a) and (b)] and without [(c) and (d)] coincidence with evaporated protons. Overlapping excitation energy regions marked between two dotted lines are used for determining the desired cross sections.

Eq. (1). Following the method described in Refs. [11,12], the ratio of the compound nuclear reaction cross section at the same excitation energy of $\sigma^{^{53}\mathrm{Mn}(n,xp)}$ and $\sigma^{^{60}\mathrm{Ni}(n,xp)}$ has been obtained using the following relation:

$$\frac{\sigma^{^{53}\mathrm{Mn}(n,xp)}(E^*)}{\sigma^{^{60}\mathrm{Ni}(n,xp)}(E^*)} = \frac{\sigma^{\mathrm{CN}}_{n+^{53}\mathrm{Mn}}(E^*)}{\sigma^{\mathrm{CN}}_{n+^{60}\mathrm{Ni}}(E^*)} \frac{P_p^{^{54}\mathrm{Mn}}(E^*)}{P_p^{^{61}\mathrm{Ni}}(E^*)}. \quad (2)$$

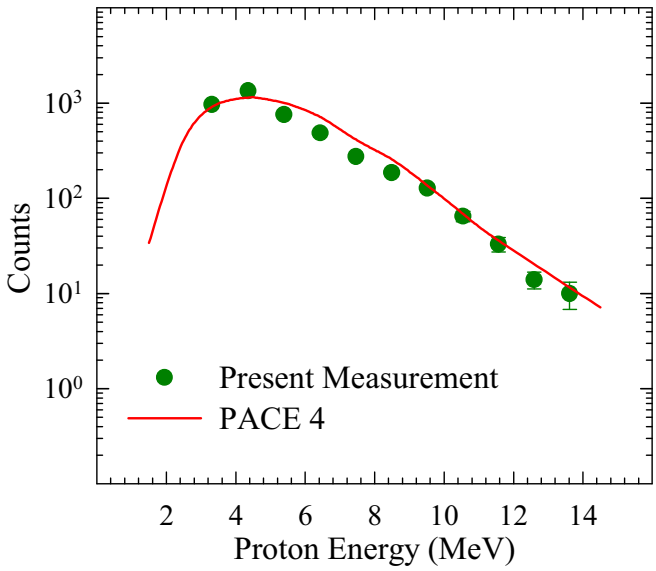

FIG. 7. Measured proton energy spectrum in coincidence with PLF α particles for the ^{6}Li + ^{52}Cr reaction at E_{lab} = 33.0 MeV corresponding to a compound nucleus excitation energy of ≈22.5 MeV. The prediction by the statistical model code PACE4, normalized to the data, is shown as a continuous line.

The cross-section values for reference reaction ^{60}Ni(n, xp) ($\sigma^{^{60}\mathrm{Ni}(n,xp)}$) as a function of excitation energy are taken from JENDL-4.0 [13] evaluation that closely reproduces the available experimental data taken from EXFOR [14] as shown in Fig. 11 of Ref. [9]. The neutron capture cross sections leading to compound systems ^{54}Mn* and ^{61}Ni* ($\sigma^{\mathrm{CN}}_{n+^{53}\mathrm{Mn}}$ and $\sigma^{\mathrm{CN}}_{n+^{60}\mathrm{Ni}}$) are calculated by using the TALYS-1.8 [15] statistical model code in the excitation energy range of E^* = 17–25 MeV. The cross sections for the ^{53}Mn(n, xp) reaction have been determined over the excitation energy range of E^* = 17–25 MeV in steps of 1.0-MeV bin using the neutron capture cross sections along with measured proton decay probabilities for compound systems ^{54}Mn* and ^{61}Ni* and the cross sections for the reference reaction ^{60}Ni(n, xp) for each excitation energy bin. The excitation energy range was then converted to the equivalent neutron energy range of E_n = 8.2–16.4 MeV using the expression $E_n = \frac{A+1}{A}(E^* - S_n)$ where $A + 1$ (=54) is the mass number and S_n (=8.938 MeV) is the neutron separation energy of the compound nucleus ^{54}Mn. The observed ^{53}Mn(n, xp) reaction cross sections as a function of incident neutron energy are shown in Fig. 8 as filled circles. It may be noted that the difference between the spin populated in the compound nuclei formed in the neutron

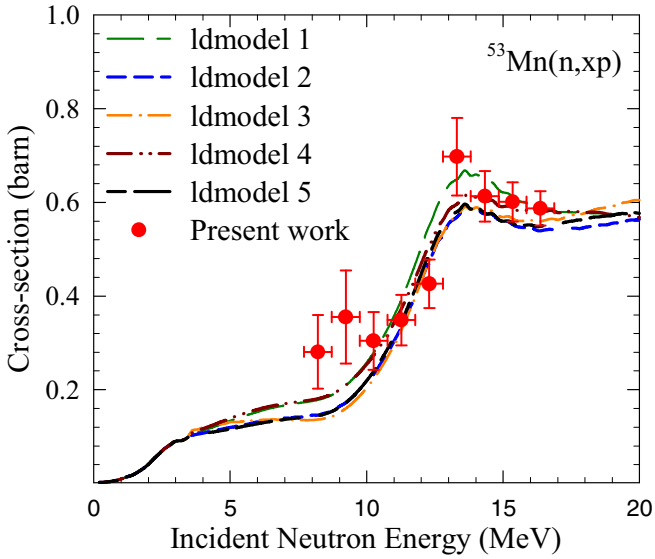

FIG. 8. The experimental cross sections for the ^{53}Mn(n, xp) reactions have been compared with TALYS-1.8 predictions using different level-density models with default parameters.

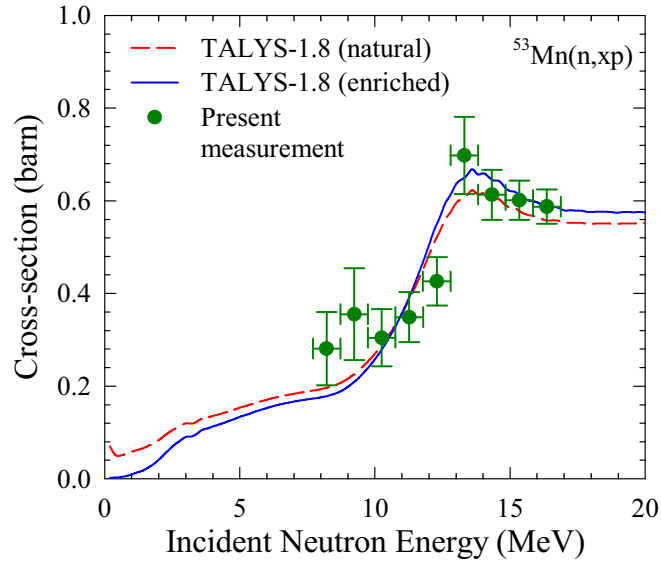

FIG. 9. The experimental cross sections for the ^{53}Mn(n, xp) reactions have been compared with TALYS-1.8 statistical model calculations for the cases of enriched and natural targets as discussed in the text.

induced reactions and the corresponding surrogate reactions in the present paper were found to be $\approx 4\hbar < 10\hbar$, satisfying the condition [16,17] for the validity of the surrogate ratio method.

III. RESULTS AND DISCUSSIONS

Statistical model calculations have been carried out for the quantitative understanding of the ^{53}Mn(n, xp) cross-section data employing the TALYS-1.8 code within the framework of the Hauser-Feshbach statistical model [18]. The ^{53}Mn(n, p), ^{53}Mn(n, np), and ^{53}Mn$(n, 2p)$ reactions with energy thresholds of 0.0, 6.685, and 9.939 MeV are possible sources of proton emission contributing to the total ^{53}Mn(n, xp) cross section in the measured excitation energy region. In the calculations, all the required inputs, such as nuclear masses, discrete energy levels, transmission coefficients, and nuclear level densities of nuclides involved have been taken from the latest reference input parameter library RIPL-3 [19]. The global optical model potentials for a neutron and a proton proposed by Koning and Delaroche [20] have been used to calculate the transmission coefficients. The TALYS-1.8 predictions for ^{53}Mn(n, xp) cross sections for various level-density options [21,22] are shown in Fig. 8 along with the present experimental data for a comparison. The TALYS-1.8 predictions compare reasonably well with experimental data for any of the level-density parameter options from ldmodel-1 to ldmodel-5. In all these cases, both discrete and continuum level densities of the initial- as well as the final-state nuclei have been considered by using the option "disctable-2" that corresponds to the experimental level densities available in the RIPL database. The calculations have also been performed using option "disctable-3" corresponding to the theoretical level densities based on the "constant temperature + Fermi gas model." The predictions of TALYS-1.8 with option disctable-2 compares well with the experimental data. Whereas, the predictions with option disctable-3 are higher in magnitude. Hence, all the calculations have been performed using the experimental level densities (option disctable-2).

The ^{53}Mn(n, xp) reaction cross sections calculated using TALYS-1.8 for the enriched target (100% ^{52}Cr) and natural Cr target are shown in Fig. 9. The natural Cr target has the abundances of ^{50}Cr ($\approx$4.345%), ^{52}Cr ($\approx$ 83.79%), ^{53}Cr ($\approx$9.5%), and ^{54}Cr ($\approx$2.36%) leading to contributions from the ^{51}Mn(n, xp), ^{53}Mn(n, xp), ^{54}Mn(n, xp),

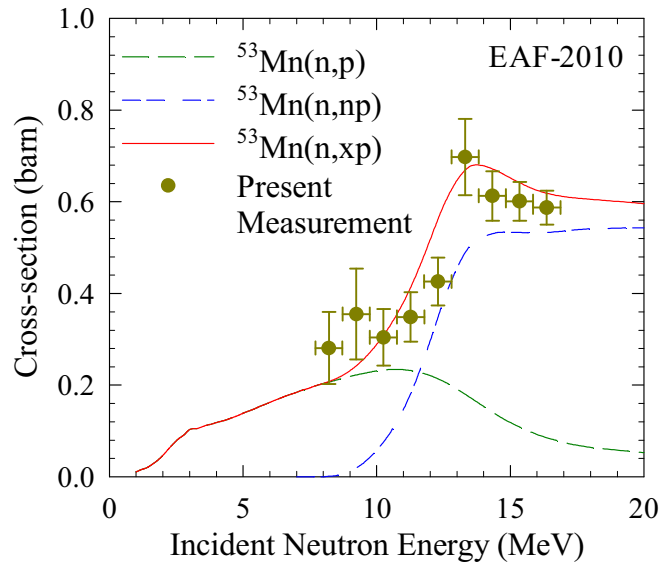

FIG. 10. The experimental ^{53}Mn(n, xp) cross sections as a function of equivalent neutron energy along with (n, p), (n, np), and (n, xp) of ^{53}Mn from EAF-2010 evaluation.

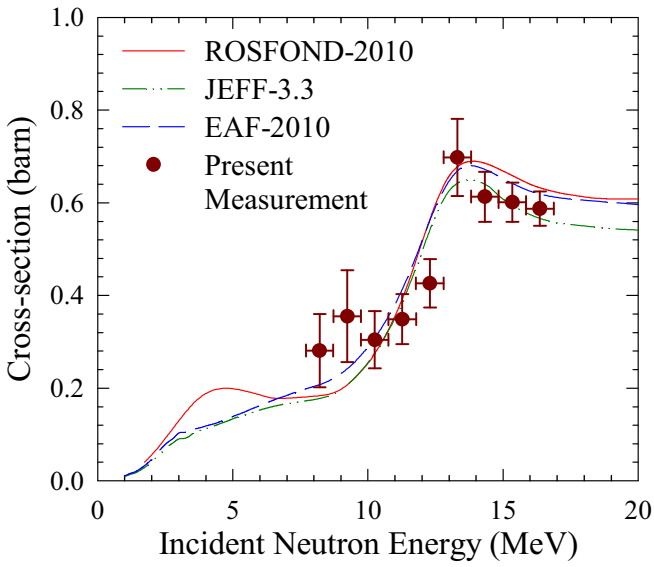

FIG. 11. The experimental ^{53}Mn(n, xp) cross sections as a function of equivalent neutron energy along with the ones from various nuclear data libraries.

and ^{53}Mn(n, xp) reactions, respectively. For each α-energy bin, the excitation energy, equivalent neutron energy, and (the n, xp) cross section corresponding to each isotope have been calculated using TALYS-1.8. Finally, the cross sections are added with the weight factors equal to their abundance in the natural target. The difference in the results of (n, xp) cross sections obtained using natural (Cr) and enriched (^{52}Cr) targets is estimated to be maximum up to 9%.

The experimental ^{53}Mn(n, xp) cross sections have been compared with cross sections of individual proton emission channels, such as ^{53}Mn(n, p) and ^{53}Mn(n, np) along with their sum [^{53}Mn(n, xp)] as predicted by the EAF-2010 [23] data library in Fig. 10. The cross sections for the ^{53}Mn$(n, 2p)$ proton emission channel are found to be negligibly small for incident neutron energy up to 20 MeV. Hence, the cross section for this channel has not been shown in Fig. 10.

Finally, the cross sections determined for the ^{53}Mn(n, xp) reactions in the present surrogate measurements have been compared with predictions of evaluated nuclear data libraries: EAF-2010, ROSFOND-2010 [24], and JEFF-3.3 [25] as shown in Fig. 11. Results from the above evaluations are observed to be in very good agreement with the measured cross sections in the equivalent neutron energy range of 8.2–16.4 MeV.

IV. SUMMARY AND CONCLUSION

To summarize, we have determined the ^{53}Mn(n, xp) cross sections by employing the surrogate reaction ratio method. The ^{52}Cr(^{6}Li, α)^{54}Mn* and ^{59}Co(^{6}Li, α)^{61}Ni* transfer reactions have been used to populate ^{54}Mn* and ^{61}Ni* compound systems, which are the surrogates of the $n + {}^{53}$Mn and $n + {}^{60}$Ni reactions, respectively. The proton decay probabilities are measured in the excitation energy range of 17–25 MeV for both compound systems. The ^{53}Mn(n, xp) cross sections in the equivalent neutron energy of 8.2–16.4 MeV have been determined within the framework of surrogate reaction ratio method using ^{60}Ni(n, xp) cross sections as the reference. The present experimental cross sections of ^{53}Mn(n, xp) have been compared with the predictions of the TALYS-1.8 code and data evaluation libraries EAF-2010, ROSFOND-2010, and JEFF-3.3. The experimental cross sections are found to be well explained by both the predictions of TALYS-1.8 code as well as the results obtained from various data evaluation libraries, such as EAF-2010, ROSFOND-2010, and JEFF-3.3 in the equivalent neutron energy range measured in the present paper.

ACKNOWLEDGMENTS

We are thankful to the operating staff of the BARC-TIFR Pelletron Accelerator for smooth operation of the accelerator during the experiment.

[1] Report summary of European facility for innovative reactor and transmutation neutron data, Project report on 2013, Belgium, id:211499 [https://cordis.europa.eu/project/rcn/88553/reporting/en] (unpublished).
[2] H. Iida, V. Khripunov, L. Petrizzi, and G. Federici, Nuclear Analysis Report (NAR), Nuclear Analysis Group, ITER Naka & Garching Joint Work Sites, ITER Report No. G 73 DDD 2W 0.2, 2004 (unpublished).
[3] M. R. Gilbert, S. Dudarev, S. Zheng, L. W. Packer, and J. Sublet, Nucl. Fusion **52**, 083019 (2012).
[4] S. Fetter, E. T. Cheng, and F. M. Mann, Fusion Eng. Des. **6**, 123 (1988).
[5] A. Wallner *et al.*, J. Korean Phys. Soc. **59**, 1378 (2011).
[6] R. A. Forrest, Fusion Eng. Des. **81**, 2143 (2006).
[7] R. A. Forrest, A. Tabasso, C. Danani, S. Jakhar, and A. K. Shaw, *Handbook of Activation Data Calculated Using EASY-2007* (EURATOM/UKAEA Fusion Association, Abingdon, U.K., 2009), p. 168.
[8] B. Pandey *et al.*, Phys. Rev. C **93**, 021602(R) (2016).
[9] J. Pandey *et al.*, Phys. Rev. C **99**, 014611 (2019).
[10] A. Gavron, Phys. Rev. C **21**, 230 (1980).
[11] B. K. Nayak, A. Saxena, D. C. Biswas, E. T. Mirgule, B. V. John, S. Santra, R. P. Vind, R. K. Choudhury, and S. Ganesan, Phys. Rev. C **78**, 061602(R) (2008).
[12] J. E. Escher, J. T. Burke, F. S. Dietrich, N. D. Scielzo, I. J. Thompson, and W. Younes, Rev. Mod. Phys. **84**, 353 (2012).
[13] EXFOR data library [https://wwwndc.jaea.go.jp/jendl/j40/j40.html].
[14] EXFOR data library [https://www-nds.iaea.org/exfor/exfor.htm].
[15] A. J. Koning, S. Hilaire, and S. Goriely, *TALYS-1.8, A Nuclear Reaction Program, User Manual* (NRG, Petten, The Netherlands, 2015), available with TALYS-1.8 code distribution at https://www.talys.eu
[16] S. Chiba and O. Iwamoto, Phys. Rev. C **81**, 044604 (2010).

[17] S. Chiba, O. Iwamoto, and Y. Aritomo, Phys. Rev. C **84**, 054602 (2011).
[18] W. Hauser and H. Feshbach, Phys. Rev. **87**, 366 (1952).
[19] R. Capote *et al.*, Nucl. Data Sheets **110**, 3107 (2009).
[20] A. J. Koning and J. P. Delaroche, Nucl. Phys. **A713**, 231 (2003).
[21] S. Hilaire, M. Girod, S. Goriely, and A. J. Koning, Phys. Rev. C **86**, 064317 (2012).
[22] S. Goriely, S. Hilaire, and A. J. Koning, Phys. Rev. C **78**, 064307 (2008).
[23] EAF-2010: European Activation File [http://www-nds.iaea].
[24] ROSFOND-2010: Updated Russian Library of Evaluated Neutron Data [http://www-nds.iaea.org/exfor/endf.html].
[25] JEFF-3.3: Joint Evaluated Fission and Fusion Nuclear Data Library [http://www-nds.iaea.org/exfor/endf.html].